inorganics

MDPI

Article

Unique Hydrogen Desorption Properties of $LiAlH_4$/h-BN Composites

Yuki Nakagawa *, Shigehito Isobe, Takao Ohki and Naoyuki Hashimoto

Graduate School of Engineering, Hokkaido University, N-13, W-8, Sapporo 060-8278, Japan; isobe@eng.hokudai.ac.jp (S.I.); takao-ohki@eng.hokudai.ac.jp (T.O.); hasimoto@eng.hokudai.ac.jp (N.H.)

* Correspondence: y-nakagawa@eng.hokudai.ac.jp; Tel.: +81-11-706-8175

Received: 30 September 2017; Accepted: 23 October 2017; Published: 25 October 2017

Abstract: Hexagonal boron nitride (h-BN) is known as an effective additive to improve the hydrogen de/absorption properties of hydrogen storage materials consisting of light elements. Herein, we report the unique hydrogen desorption properties of $LiAlH_4$/h-BN composites, which were prepared by ball-milling. The desorption profiles of the composite indicated the decrease of melting temperature of $LiAlH_4$, the delay of desorption kinetics in the first step, and the enhancement of the kinetics in the second step, compared with milled $LiAlH_4$. Li_3AlH_6 was also formed in the composite after desorption in the first step, suggesting h-BN would have a catalytic effect on the desorption kinetics of Li_3AlH_6. Finally, the role of h-BN on the desorption process of $LiAlH_4$ was discussed by comparison with the desorption properties of $LiAlH_4$/X (X = graphite, LiCl and LiI) composites, suggesting the enhancement of Li ion mobility in the $LiAlH_4$/h-BN composite.

Keywords: alanate; h-BN; hydrogen storage; catalyst; Li ion mobility

1. Introduction

Hydrogen storage is a key technology for a future hydrogen energy society [1]. However, it is still challenging to develop high performance hydrogen storage materials with high hydrogen density, fast de/absorption kinetics, and high cycle stability under moderate temperature and pressure conditions [2,3]. $LiAlH_4$ is one of the most promising hydrogen storage materials because of its high hydrogen capacity and relatively low desorption temperature [4]. The hydrogen desorption process of $LiAlH_4$ is described as follows:

Melting:

$LiAlH_4(s) \rightarrow LiAlH_4(l)$ Endothermic (150–175 °C)

Decomposition in the first step:

$3LiAlH_4(l) \rightarrow Li_3AlH_6(s) + 2Al + 3H_2$ Exothermic (150–200 °C, 5.3 mass % H_2)

Decomposition in the second step:

$Li_3AlH_6(s) \rightarrow 3LiH + Al + 3/2H_2$ Endothermic (200–270 °C, 2.6 mass % H_2)

The decomposition in the first step is an exothermic reaction with a ΔH of -10 kJ·mol^{-1} H_2, indicating the reversibility of this step is believed to be thermodynamically difficult [4,5]. In the second step, Li_3AlH_6 decomposes in an endothermic reaction with a ΔH of 25 kJ·mol^{-1} H_2 [4]. Thus, the hydrogenation of LiH/Al to Li_3AlH_6 is thermodynamically possible.

One of the strategies for improving the properties of hydrogen storage materials is the addition of catalysts/dopants [6]. Ti or its compounds are well-known catalysts for the kinetics of alanate [7–9]. Since Bogdanović et al. reported an absence of hysteresis and nearly horizontal pressure plateaus in the $TiCl_3$-doped $NaAlH_4$ [7], many researchers have studied complex hydrides including alanate

as potential reversible hydrogen storage materials. In the case of $LiAlH_4$, the improved desorption kinetics was reported by the doping of Ti catalyst using mechanically milling [10–12]. Recent study also reported a single step hydrogen release of $LiAlH_4$, which was induced by the synergetic effects of Ti catalytic coating and nanosizing effects [13]. Although the rehydrogenation of the desorbed material was not achieved in the milled sample, the regeneration of $LiAlH_4$ from LiH and Ti-catalyzed Al was possible through the solution synthesis approach using THF and Me_2O [14–16].

Hexagonal boron nitride (h-BN) is known as an effective additive for chemical hydride and complex hydride systems. For instance, NH_3BH_3/h-BN composite released hydrogen at low temperature with minimum induction time and less exothermicity [17]. The remarkable hydrogen de/absorption properties were also achieved in the milled $LiBH_4$/h-BN composites [18,19]. The 30 mol % h-BN doped $LiBH_4$ composite started to release hydrogen from 180 °C, which was 100 °C lower than the onset hydrogen desorption temperature of ball-milled $LiBH_4$ [18]. For the 75 mol % h-BN doped $LiBH_4$ composite, the on-set desorption temperature of $LiBH_4$ was reduced to 175 °C and the peak desorption temperature was reduced by 80 °C compared with milled $LiBH_4$ [19]. Furthermore, under moderate rehydrogenation conditions of 400 °C and 10 MPa H_2 pressure, the dehydrogenation capacity of the composite maintained 3.1 mass % within three cycles, which was very close to its theoretical capacity. It was assumed that the excellent rehydrogenation property of $LiBH_4$ would be related with the enhanced hydrogen and lithium diffusion capability by the nanoscale h-BN, which was synthesized by ball-milling of h-BN at 490 rpm for 20 h [19]. The enhancement of Li^+ and/or H^- diffusion by adding h-BN was firstly reported in the $LiNH_2$/LiH system [20]. Hydrogen was fully desorbed from the $LiNH_2$/LiH/h-BN composite in less than 7 h, whereas the $LiNH_2$/LiH composite desorbed hydrogen in several days. They proposed that h-BN is an efficient catalyst that improves Li^+ diffusion and hence the kinetics of the reaction between $LiNH_2$ and LiH [20]. The mobility of Li^+ ions between LiH and $LiNH_2$ was also enhanced by adding $LiTi_2O_4$ catalyst [21].

Thus, h-BN has attracted much attention as an effective additive to improve the hydrogen de/absorption kinetics of hydrogen storage materials, especially for complex hydrides. However, the addition of h-BN to the alanate system has rarely been reported. In the present study, $LiAlH_4$/h-BN composites were synthesized by planetary ball-milling and their hydrogen desorption properties were analyzed. Also, the desorption process of the composite was investigated by using XRD and FT-IR. Finally, the role of h-BN to the desorption properties of $LiAlH_4$ was discussed by comparison with those of $LiAlH_4$/X (X = graphite, LiCl and LiI) composites.

2. Results

Hydrogen desorption properties of $LiAlH_4$/h-BN composites were analyzed by using TG-DTA-MS. Figure 1 shows the DTA and MS (H_2, m/z = 2) profiles of the composites. As shown in Figure 1a, ball-milled $LiAlH_4$ (denoted as 0 mass % in Figure 1) started to melt around 150 °C followed by hydrogen desorption in two steps below 250 °C. In the case of $LiAlH_4$/h-BN composites, desorption profiles were clearly changed compared with $LiAlH_4$. First, the melting temperature (T_m) of $LiAlH_4$ was decreased by adding h-BN. For instance, in the 40 mass % h-BN composite, DTA peak value of T_m was 151 °C, which was 11 °C lower than that of milled $LiAlH_4$. Second, the hydrogen desorption temperature (T_d) in the first step was slightly increased by h-BN addition. As shown in Figure 1b, T_d in the first step became high value with the increasing amount of h-BN. Third, the desorption kinetics in the second step was improved by adding h-BN. As shown in Figure 1b, the desorption peak in the second step became sharp as the amount of h-BN increased up to 14 mass %. However, the peak shape became broad in the 40 mass % h-BN composite, suggesting the addition of too much amount of h-BN could have negative effect on improving the kinetics. Figure 2 shows the TG profiles of $LiAlH_4$/h-BN composites. The total mass loss from TG profile of ball-milled $LiAlH_4$ was 7.7 mass %, which was in good agreement with the theoretical hydrogen desorption amount of $LiAlH_4$ (7.9 mass %) [4]. The hydrogen mass loss of 6.9 mass %, 5.8 mass %, and 3.5 mass % were calculated

from the profiles of 4 mass %, 14 mass %, and 40 mass % h-BN composites, respectively. It is noted that theoretical hydrogen desorption capacities of these composites were 7.6 mass %, 6.8 mass %, and 4.7 mass %, respectively, when only considering the hydrogen desorption from $LiAlH_4$. Thus, the experimental values of hydrogen desorption amounts were slightly lower than the theoretical values. This result could originate from the hydrogen desorption during ball-milling or the formation of new H-containing solid compound by the reaction between $LiAlH_4$ and h-BN.

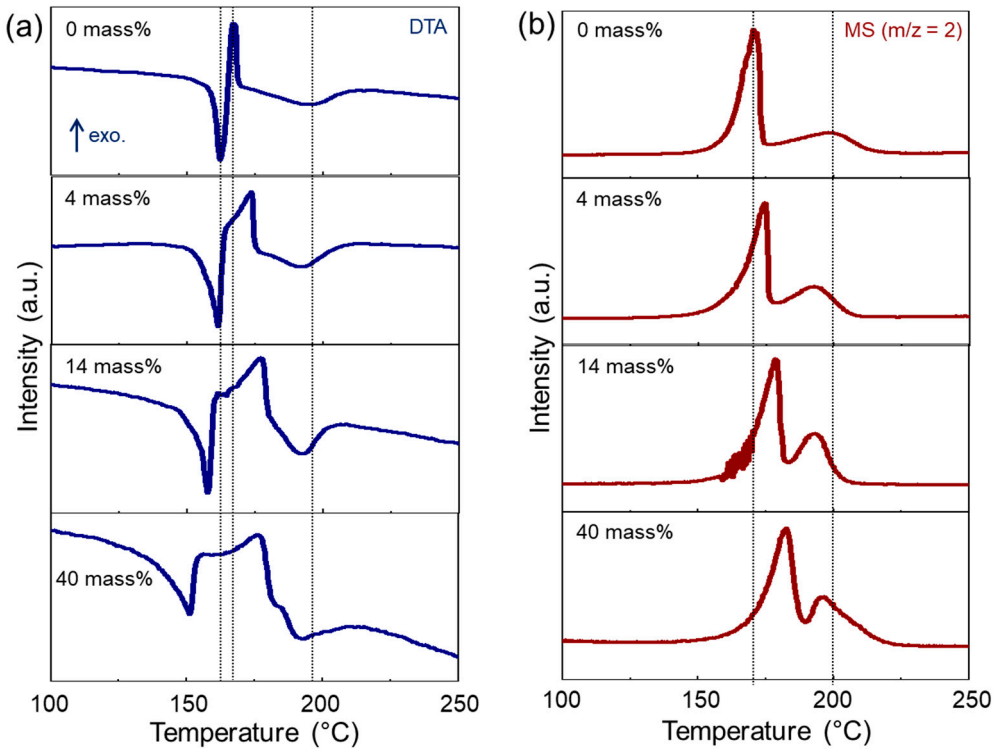

Figure 1. Hydrogen desorption profiles of $LiAlH_4/x$ mass % h-BN (x = 0, 4, 14, 40) composites: (**a**) DTA and (**b**) MS (m/z = 2, H_2) profiles. Heating rate was 5 °C·min^{-1}.

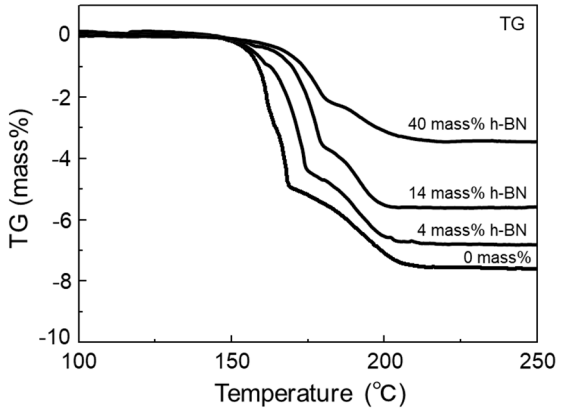

Figure 2. TG profiles of $LiAlH_4/x$ mass % h-BN (x = 0, 4, 14, 40) composites. Heating rate was 5 °C·min^{-1}.

To investigate the interaction between $LiAlH_4$ and h-BN, XRD, and FT-IR measurements were performed for the $LiAlH_4$/h-BN composites. Also, the particle size of composite was observed by using SEM and TEM. Figure 3a shows the XRD profiles of the milled $LiAlH_4$ and $LiAlH_4$/h-BN composites. Only $LiAlH_4$ and h-BN phases were observed in the profiles of the composites. Although

the diffraction peaks of $LiAlH_4$ were slightly broadened by h-BN addition, the clear relationship between the broadning and the amount of h-BN was not observed. Figure 3b,c shows the XRD profiles of the milled $LiAlH_4$ and 40 mass % h-BN composite after hydrogen desorption. The 40 mass % h-BN composite formed the similar reaction products compared with $LiAlH_4$. In other words, Li_3AlH_6 and Al were formed after the hydrogen desorption in the first step, and LiH and Al were formed after the second step. The phase of h-BN was also clearly observed after hydrogen desorption. Broad diffraction peaks around 20° and 27° originate from the polyimide film and grease to prevent the sample oxidation. Figure 4 shows SEM and TEM images of 40 mass % h-BN composite and references. As shown in Figure 4a, the milled $LiAlH_4$ contained a lot of large particles with sizes over 10 μm. On the other hand, the 40 mass % h-BN composite showed the average particle size of a few micrometers, indicating the refinement of $LiAlH_4$ particles occurred in the composite. The submicron particles were also observed in the TEM image of the composite, as shown in Figure 4d. The size of as-received h-BN particle was around 1 μm (Figure 4b). Figure 5 shows the FT-IR spectra of 40 mass % h-BN composite and references. The as-milled composite showed the characteristic Al–H vibrations of $LiAlH_4$ [22] around 1795 cm^{-1} and 1644 cm^{-1}. Also, B–N vibrations of h-BN around 1373 cm^{-1} and 818 cm^{-1} were observed. Although the Al–H vibrations of $LiAlH_4$ disappeared after heating, the B–N vibrations of h-BN still remained. These results were consistent with the results of XRD. However, new IR absorption peak was clearly observed around 2300 cm^{-1} after heating up to 183 °C and 300 °C. Also, another new peak appeared around 1100 cm^{-1} after heating up to 300 °C. Although these peaks were not identified in this work, the peak positions were similar to those of $LiBH_4$ [23], suggesting a such kind of Li–B–H phase exist after heating up to 183 °C and/or 300 °C. The unknown peak around 2300 cm^{-1} was also observed for the IR spectra of the composite consisting of $BN^{nano}H_x$ (ball-milled h-BN under 1.0 MPa H_2 for 80 h) and LiH [24]. Thus, the formation of new H-containing solid compound could result in the slightly low hydrogen desorption amount in Figure 2. Considering the results of Figure 5, the possible new compound could be covalently functionalized h-BN species. The details were explained in the next discussion part.

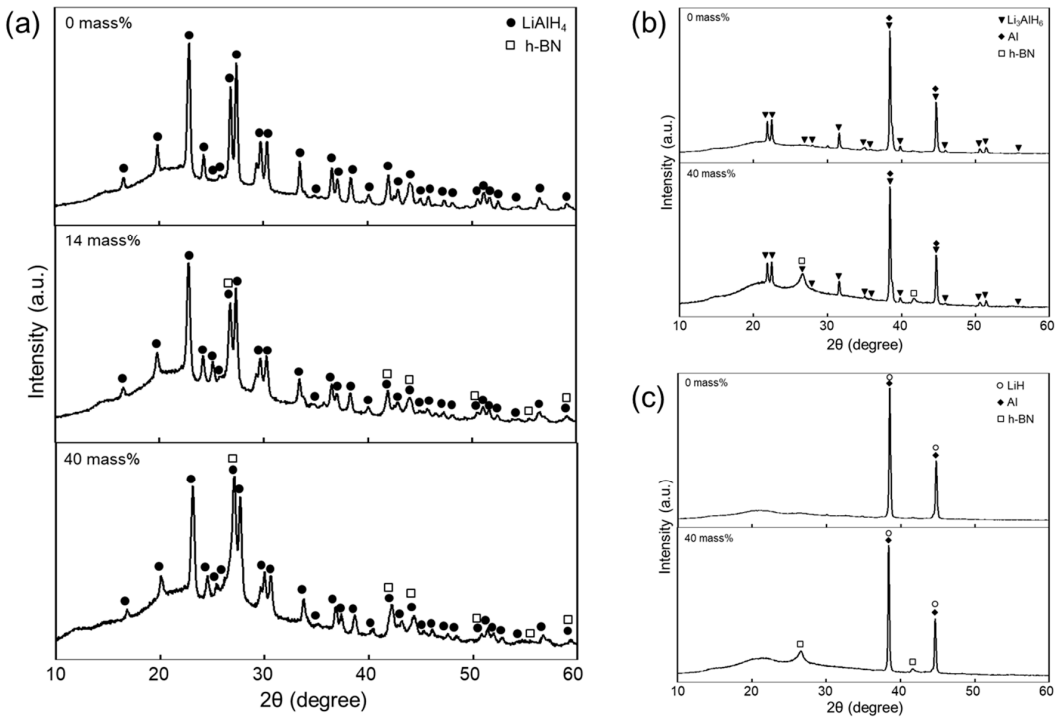

Figure 3. XRD profiles of $LiAlH_4/x$ mass % h-BN (x = 0, 14, 40) composites: (**a**) after ball-milling; (**b**) after desorption in the first step; and (**c**) after desorption in the second step. The heating rate was 5 °C·min^{-1}.

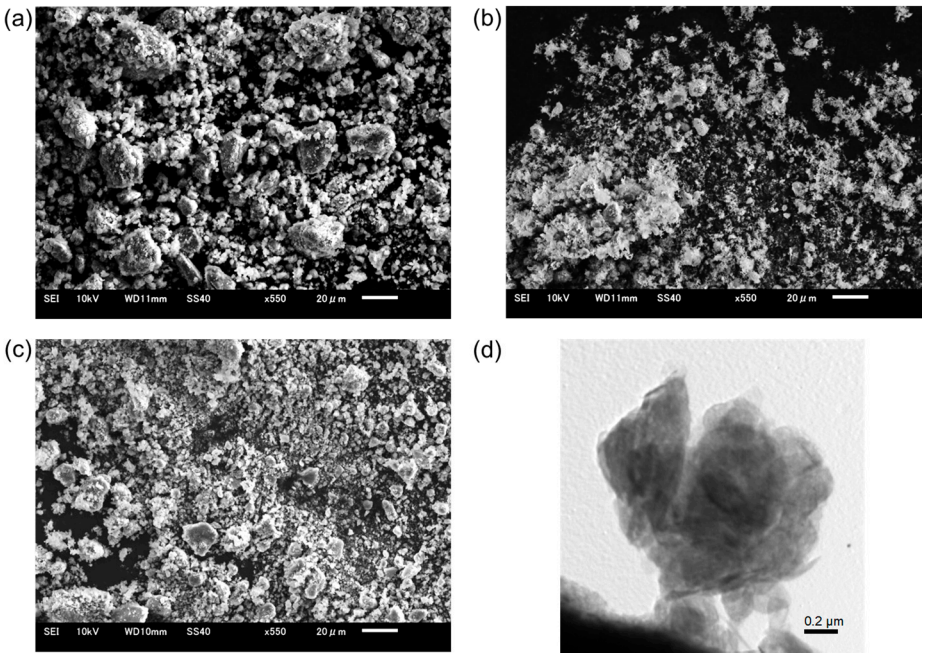

Figure 4. SEM images of (**a**) milled $LiAlH_4$; (**b**) h-BN; (**c**) $LiAlH_4$/40 mass % h-BN composite after milling; and (**d**) TEM image of $LiAlH_4$/40 mass % h-BN composite after milling.

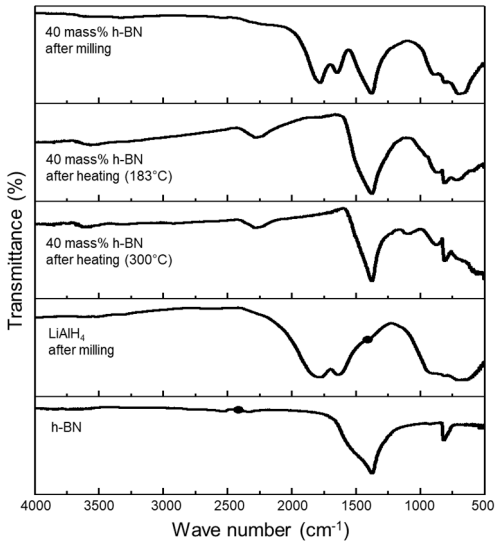

Figure 5. FT-IR spectra of $LiAlH_4$/40 mass % h-BN composite after milling and after hydrogen desorption. $LiAlH_4$ and h-BN spectra are shown as the references. Heating rate was 5 °C·min^{-1}.

As shown in the results of structural characterizaion, $LiAlH_4$/h-BN composites also formed Li_3AlH_6 as an intermediate product, indicating the similar decomposition pathway with $LiAlH_4$. Thus, h-BN would have the catalytic effect on the hydrogen desorption kinetics of Li_3AlH_6. The apparent activation energy for hydrogen desorption was calculated by using the Kissinger equation [25],

$$\ln \frac{c}{T_p^2} = -\frac{E_a}{RT_p} + \ln \frac{RA}{E_a}$$

where E_a is the apparent activation energy for hydrogen desorption, c is the heating rate, T_p is the peak temperature, R is gas constant, and A is the frequency factor. Figure 6 shows the Kissinger plots for the hydrogen desorption in the second step of 4 mass % h-BN composite. The obtained apparent activation

energy, E_a was 71.5 kJ·mol^{-1}. This value is lower than that reported for Li_3AlH_6 (92 kJ·mol^{-1}) [26], indicating the desorption kinetics was improved by adding h-BN.

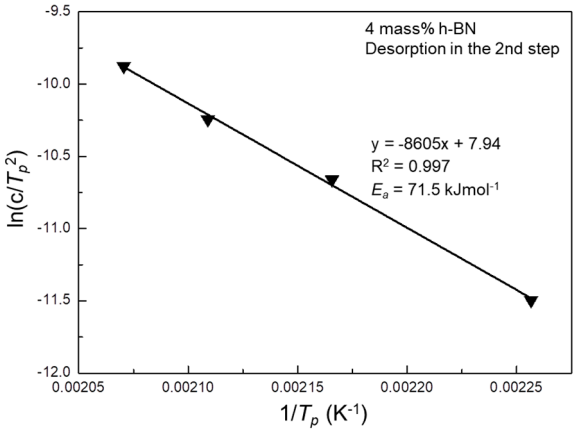

Figure 6. Kissinger plots for the hydrogen desorption in the second step of $LiAlH_4$/4 mass % h-BN composite. Heating rates were 2, 5, 8, and 12 °C·min^{-1}.

In order to understand the role of h-BN, other additives were also ball-milled with $LiAlH_4$ and their desorption properties were analyzed. The detailed results (Figure 7) and the possible role of h-BN on the desorption process were explained in the next discussion part.

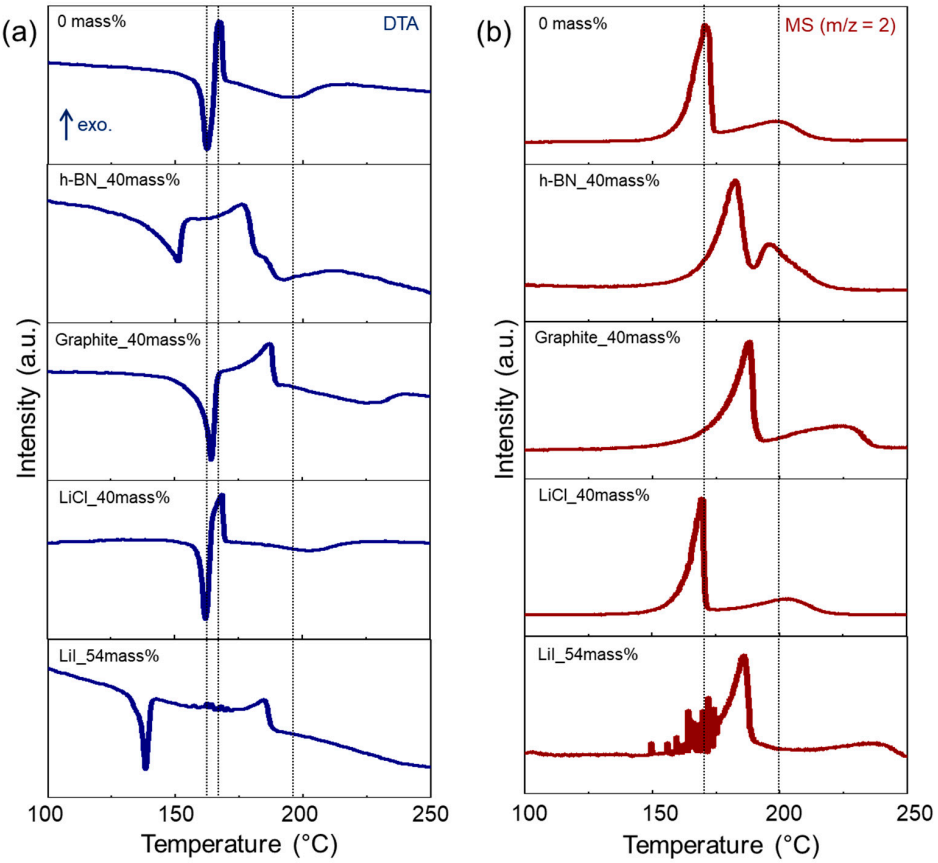

Figure 7. Hydrogen desorption profiles of $LiAlH_4$/X (X = graphite, LiCl, and LiI) composites. The profiles of milled $LiAlH_4$ and $LiAlH_4$/h-BN composites are shown as the references: (**a**) DTA and (**b**) MS (m/z = 2, H_2) profiles. Heating rate was 5 °C·min^{-1}.

3. Discussion

Figure 7 shows the DTA and MS profiles of $LiAlH_4$/X (X = graphite, LiCl, and LiI) composites. The profiles of $LiAlH_4$ and $LiAlH_4$/h-BN composites are also shown as the references. Graphite was selected as an additive because this compound has a structure similar to h-BN. In spite of its similar structure, hydrogen desorption properties were different from those of h-BN. In the case of $LiAlH_4$/graphite composite, the melting temperature was similar to ball-milled $LiAlH_4$. Also, the desorption kinetics in the second step seemed to be delayed, whereas that of $LiAlH_4$/h-BN was enhanced. Since the both graphite and h-BN are hard materials, the refinement of $LiAlH_4$ particles would occur during the ball-milling process. However, the different desorption profiles were obtained between h-BN and graphite composite, suggesting just the refinement of particles cannot explain this difference. Although the desorption properties of nanoconfined $LiAlH_4$ into graphite with high surface area was reported in the previous study [27], the profiles of graphite composite in this study seemed to be different from those profiles.

Also, LiCl and LiI were selected as additives. Aguey-Zinsou et al. reported that h-BN would enhance the Li ion mobility across the interface of $LiNH_2$ and LiH [20]. Thus, the enhancement of Li ion mobility could be one of the reasons for the unique hydrogen desorption properties of $LiAlH_4$/h-BN composites. Oguchi et al. reported the Li ion conductivity of Li_3AlH_6/LiI composite at 120 °C was much higher than that of Li_3AlH_6, but that of Li_3AlH_6/LiCl at 120 °C was the similar value compared with Li_3AlH_6 [28]. Their results suggest that LiI additive would be effective for increasing the Li ion mobility of $LiAlH_4$, but LiCl would not be effective near the decomposition temperature range of $LiAlH_4$. As shown in Figure 7, the desorption profiles of LiCl composite was similar to those of milled $LiAlH_4$. On the other hand, those of LiI composite showed the decrease of melting temperature and the delay of the first desorption reaction, which was consistent with the results of h-BN composite. This comparative result suggests that Li ion conductivity would increase in the $LiAlH_4$/h-BN composite. The kinetics in the second step wasdelayed in the LiI composite. The possible origin of the high conductivity of $LiAlH_4$ is the anion substitution from complex anion to I^- [28], which partially took place in the case of $LiBH_4$ [29]. Thus, the high decomposition temperature in the second step could originate from the formation of stable solid solution similar to $LiBH_4$–LiI(LiCl) system [29–33]. For clarifying the total desorption process of these composites, the detailed mechanistic study is needed. The analysis of Li ion conductivity of $LiAlH_4$/h-BN composite is currently in progress.

As shown in Figure 1, all the $LiAlH_4$/h-BN composites showed the melting of $LiAlH_4$. This phenomenon was different from the case of $LiAlH_4$ catalyzed by transition metal (Ti, Fe, Co, Nb, etc. [34–36]), which can release hydrogen below the melting temperature. Thus, h-BN would have little interaction with complex anion of $[AlH_4]^-$, whereas transition metal like Ti would destabilize the covalent Al–H bond of complex anion as Sandrock et al. suggested [8]. According to the proposed mechanism by Atakli et al. [37], Li_3AlH_6 is formed by transferring the alkali cation and a hydrogen anion from the two neighboring alanate molecules to central one. In this context, the diffusion distance of Li^+ seems to be very short to form Li_3AlH_6, suggesting Li^+ diffusion would not be the rate-limiting step in the desorption of $LiAlH_4$ in the first step. On the contrary, the desorption properties of h-BN and LiI composite suggested the excess enhancement of Li^+ ion mobility might be related to delaying the formation of Li_3AlH_6. First-principle DFT studies also suggested the formation and migration of $[AlH_4]^-$ vacancy would be the rate-limiting step in the decomposition of $LiAlH_4$ [38]. In the second decomposition step, it was proposed that three LiH are formed from Li_3AlH_6, leaving AlH_3, which spontaneously desorbs hydrogen [37]. Thus, the enhanced mobility of Li^+ may help the destabilization of complex anions to improve the hydrogen desorption kinetics.

As shown in Figure 5, the presence of new bonds similar to those of $LiBH_4$ or ball-milled h-BN with LiH suggests that covalently functionalized h-BN species could be formed after heating the $LiAlH_4$/h-BN composites. It is known that ball-milling of h-BN with a lot of different materials can generate functionalized h-BN nanosheets [39]. For instance, a one-step method for the preparation and functionalization of few-layer BN was developed based on urea-assisted solid exfoliation of

commercially available h-BN [40]. Such kind of functionalized BN nanosheets are attractive for a lot of applications such as polymer matrix composites [41], ion conductors [42], and hydrogen storage [43]. Further investigations of $LiAlH_4$/h-BN composites could pave the way for the covalent functionalization of h-BN nanosheets by interaction with $LiAlH_4$.

4. Materials and Methods

4.1. Synthesis of $LiAlH_4$/X Composites

All samples were handled in an Ar-filled glovebox with O_2 and H_2O levels below 2 ppm. $LiAlH_4$ (95%, Sigma-Aldrich, Tokyo, Japan), h-BN (98%, Sigma-Aldrich), graphite (99.99%, Kojundo Chemical Lab., Sakado, Japan), LiCl (99.99%, Sigma-Aldrich) and LiI (99.9%, Sigma-Aldrich) were used as starting materials. The $LiAlH_4$/X (X = h-BN, graphite, LiCl and LiI) composites were synthesized by using planetary ball-milling apparatus (Fritsch Pulverisette 7, Yokohama, Japan) with 20 stainless balls (7 mm in diameter) and 300 mg samples (ball: powder mass ratio = 70: 1). The milling pot was equipped with a quick connector for vacuuming and introducing H_2 gas. The milling was performed under 0.1 MPa H_2 atmosphere with 400 rpm for 2 h with four cycles of 30/15 min operation/interval per each cycle. Also, the milled $LiAlH_4$ was prepared under the same milling conditions for comparison.

4.2. Characterization

Hydrogen desorption properties of the composites were examined by a thermogravimetry and differential thermal analysis equipment (TG-DTA, Bruker, 2000SA, Yokohama, Japan) connected to a mass spectrometer (MS, ULVAC, BGM-102, Chitose, Japan). The desorbed gases were carried from TG-DTA to MS through a capillary by 300 $mL \cdot min^{-1}$ stream of high purity He as a carrier gas. The samples were heated from room temperature to 300 °C with a heating rate of 5 $°C \cdot min^{-1}$. Structural properties were investigated by powder X-ray diffraction (XRD) measurements (Philips, X'Pert Pro with Cu Kα radiation, Amsterdam, The Netherlands), where all the samples were covered with a polyimide sheet (Kapton, The Nilaco Co., Ltd., Tokyo, Japan) in the glovebox to avoid oxidation during the measurement. Morphology of the composites was observed using scanning electron microscope (SEM, JEOL, JSM-6510LA, Tokyo, Japan) and transmission electron microscope (TEM, JEOL, JEM-2010, Tokyo, Japan). For TEM observations, the samples were dispersed on a molybdenum micro-mesh grid. Fourier transform infrared spectrometer (FT-IR, JASCO, FT/IR 660Plus, Tokyo, Japan) was operated to investigate chemical bonds in the composites. Each sample was put between KBr plates and pressed for measurement.

5. Conclusions

Hydrogen desorption properties of the ball-milled $LiAlH_4$/h-BN composites were investigated. Compared with milled $LiAlH_4$, the composites showed the different desorption profiles, where the decrease of melting temperature (T_m), the delay of desorption kinetics in the first step and the enhancement of the kinetics in the second step were observed. In the 40 mass % h-BN composite, the DTA peak value of T_m was 151 °C, which was 11 °C lower than that of milled $LiAlH_4$. The $LiAlH_4$/h-BN composite formed Li_3AlH_6 after desorption in the first step similar to $LiAlH_4$. Thus, h-BN would have a catalytic effect on the desorption kinetics of Li_3AlH_6. The apparent activation energy in the second step desorption was 71.5 $kJ \cdot mol^{-1}$ for the 4 mass % h-BN composite. From SEM and TEM observations, the refinement of $LiAlH_4$ particle was confirmed in the 40 mass % h-BN composite. The particle size of the composite was around a few micrometers. The hydrogen mass loss of the composite was slightly lower than the theoretical value. The new chemical bond similar to Li–B–H species was observed in the FT-IR spectra of the 40 mass % h-BN composite after the desorption. This result suggested covalently functionalized h-BN nanosheets could be formed in the composite. Finally, the desorption properties of $LiAlH_4$/h-BN composite were compared with those of

$LiAlH_4$/X (X = graphite, LiCl, and LiI) composites, suggesting the enhancement of Li ion mobility in the $LiAlH_4$/h-BN composite compared with $LiAlH_4$. The present work first demonstrates the effect of h-BN addition on the hydrogen desorption properties of alanate.

Acknowledgments: A part of this study was conducted at "Joint-use facilities: Laboratory of Nano-Micro Material Analysis, Laboratory of XPS Analysis, and the Open Facility" at Hokkaido University, supported by the "Material Analysis and Structure Analysis Open Unit (MASAOU)" and "Nanotechnology Platform" program of the Ministry of Education, Culture, Sports, Science and Technology (MEXT), Japan.

Author Contributions: Yuki Nakagawa was involved in all stages of the work, including designing the work, conducting experiments, and analyzing the data; Shigehito Isobe acted as co-supervisor and was involved in the discussion of the results and work planning; Takao Ohki performed the TG-DTA-MS and XRD experiments; Naoyuki Hashimoto acted as the main supervisor and was involved in the discussion of the results; Yuki Nakagawa wrote the paper; and all the authors contributed to the revision of the paper.

Conflicts of Interest: The authors declare no conflict of interest.

References

1. Züttel, A. Materials for hydrogen storage. *Mater. Today* **2003**, *6*, 24–33. [CrossRef]
2. Lai, Q.; Paskevicius, M.; Sheppard, D.A.; Buckley, C.E.; Thornton, A.W.; Hill, M.R.; Gu, Q.; Mao, J.; Huang, Z.; Liu, H.K.; et al. Hydrogen storage materials for mobile and stationary applications: Current state of the art. *ChemSusChem* **2015**, *8*, 2789–2825. [CrossRef] [PubMed]
3. Ley, M.B.; Jensen, L.H.; Lee, Y.S.; Cho, Y.W.; Bellosta von Colbe, J.M.; Dornheim, M.; Rokni, M.; Jensen, J.O.; Sloth, M.; Filinchuk, Y.; et al. Complex hydrides for hydrogen storage—New perspectives. *Mater. Today* **2014**, *17*, 122–128. [CrossRef]
4. Orimo, S.; Nakamori, Y.; Eliseo, J.R.; Züttel, A.; Jensen, C.M. Complex hydrides for hydrogen storage. *Chem. Rev.* **2007**, *107*, 4111–4132. [CrossRef] [PubMed]
5. Jang, J.W.; Shim, J.H.; Cho, Y.W.; Lee, B.J. Thermodynamic calculation of $LiH \leftrightarrow Li_3AlH_6 \leftrightarrow LiAlH_4$ reactions. *J. Alloys Compd.* **2006**, *420*, 286–290. [CrossRef]
6. Wu, H. Strategies for the improvement of the hydrogen storage properties of metal hydride materials. *ChemPhysChem* **2008**, *9*, 2157–2162. [CrossRef] [PubMed]
7. Bogdanović, B.; Schwickardi, M. Ti-doped alkali metal aluminum hydrides as potential novel reversible hydrogen storage materials. *J. Alloys Compd.* **1997**, *253–254*, 1–9. [CrossRef]
8. Sandrock, G.; Gross, K.; Thomas, G. Effect of Ti-catalyst content on the reversible hydrogen storage properties of the sodium alanates. *J. Alloys Compd.* **2002**, *339*, 299–308. [CrossRef]
9. Gremaud, R.; Borgschulte, A.; Lohstroh, W.; Schreuders, H.; Züttel, A.; Dam, B.; Griessen, R. Ti-catalyzed $Mg(AlH_4)_2$: A reversible hydrogen storage material. *J. Alloys Compd.* **2005**, *404–406*, 775–778. [CrossRef]
10. Easton, D.S.; Schneibel, J.H.; Speakman, S.A. Factors affecting hydrogen release from lithium alanate ($LiAlH_4$). *J. Alloys Compd.* **2005**, *398*, 245–248. [CrossRef]
11. Amama, P.B.; Grant, J.T.; Shamberger, P.J.; Voevodin, A.A.; Fisher, T.S. Improved dehydrogenation properties of Ti-doped $LiAlH_4$: Role of Ti precursors. *J. Phys. Chem. C* **2012**, *116*, 21886–21894. [CrossRef]
12. Isobe, S.; Ikarashi, Y.; Yao, H.; Hino, S.; Wang, Y.; Hashimoto, N.; Ohnuki, S. Additive effects of $TiCl_3$ on dehydrogenation reaction of $LiAlH_4$. *Mater. Trans.* **2014**, *55*, 1138–1140. [CrossRef]
13. Wang, L.; Aguey-Zinsou, K.F. Synthesis of $LiAlH_4$ nanoparticles leading to a single hydrogen release step upon Ti coating. *Inorganics* **2017**, *5*, 38. [CrossRef]
14. Liu, X.; McGrady, G.S.; Langmi, H.W.; Jensen, C.M. Facile cycling of Ti-doped $LiAlH_4$ for high performance hydrogen storage. *J. Am. Chem. Soc.* **2009**, *131*, 5032–5033. [CrossRef]
15. Graetz, J.; Wegrzyn, J.; Reilly, J.J. Regeneration of lithium aluminum hydride. *J. Am. Chem. Soc.* **2008**, *130*, 17790–17794. [CrossRef] [PubMed]
16. Wang, J.; Ebner, A.D.; Ritter, J.A. Physiochemical pathway for cyclic dehydrogenation and rehydrogenation of $LiAlH_4$. *J. Am. Chem. Soc.* **2006**, *128*, 5949–5954. [CrossRef] [PubMed]
17. Neiner, D.; Karkamkar, A.; Linehan, J.C.; Arey, B.; Autrey, T.; Kauzlarich, S.M. Promotion of hydrogen release from ammonia borane with mechanically activated hexagonal boron nitride. *J. Phys. Chem. C* **2009**, *113*, 1098–1103. [CrossRef]

18. Tu, G.; Xiao, X.; Qin, T.; Jiang, Y.; Li, S.; Ge, H.; Chen, L. Significantly improved de/rehydrogenation properties of lithium borohydride modified with hexagonal boron nitride. *RSC Adv.* **2015**, *5*, 51110–51115. [CrossRef]
19. Zhu, J.; Wang, H.; Cai, W.; Liu, J.; Ouyang, L.; Zhu, M. The milled $LiBH_4$/h-BN composites exhibiting unexpected hydrogen storage kinetics and reversibility. *Int. J. Hydrog. Energy* **2017**, *42*, 15790–15798. [CrossRef]
20. Aguey-Zinsou, K.F.; Yao, J.; Guo, Z.X. Reaction paths between $LiNH_2$ and LiH with effects of nitrides. *J. Phys. Chem. B* **2007**, *111*, 12531–12536. [CrossRef] [PubMed]
21. Zhang, T.; Isobe, S.; Matsuo, M.; Orimo, S.; Wang, Y.; Hashimoto, N.; Ohnuki, S. Effect of lithium ion conduction on hydrogen desorption of $LiNH_2-LiH$ composite. *ACS Catal.* **2015**, *5*, 1552–1555. [CrossRef]
22. Ares, J.R.; Aguey-Zinou, K.F.; Porcu, M.; Sykes, J.M.; Dornheim, M.; Klassen, T.; Bormann, R. Thermal and mechanically activated decomposition of $LiAlH_4$. *Mater. Res. Bull.* **2008**, *43*, 1263–1275. [CrossRef]
23. D'Anna, V.; Spyratou, A.; Sharma, M.; Hagemann, H. FT-IR spectra of inorganic borohydrides. Spectrochim. *Acta Part A* **2014**, *128*, 902–906. [CrossRef] [PubMed]
24. Miyaoka, H.; Ichikawa, T.; Fujii, H.; Kojima, Y. Hydrogen desorption reaction between hydrogen-containing functional groups and lithium hydride. *J. Phys. Chem. C* **2010**, *114*, 8668–8674. [CrossRef]
25. Kissinger, H.E. Reaction kinetics in differential thermal analysis. *Anal. Chem.* **1957**, *29*, 1702–1706. [CrossRef]
26. Andreasen, A.; Vegge, T.; Pedersen, A.S. Dehydrogenation kinetics of as-received and ball-milled $LiAlH_4$. *J. Solid State Chem.* **2005**, *178*, 3672–3678. [CrossRef]
27. Wang, L.; Rawal, A.; Quadir, M.Z.; Aguey-Zinsou, K.F. Nanoconfined lithium aluminum hydride ($LiAlH_4$) and hydrogen reversibility. *Int. J. Hydrog. Energy* **2017**, *42*, 14144–14153. [CrossRef]
28. Oguchi, H.; Matsuo, M.; Sato, T.; Takaumura, H.; Maekawa, H.; Kuwano, H.; Orimo, S. Lithium-ion conduction in complex hydrides $LiAlH_4$ and Li_3AlH_6. *J. Appl. Phys.* **2010**, *107*, 096104. [CrossRef]
29. Maekawa, H.; Matsuo, M.; Takamura, H.; Ando, M.; Noda, Y.; Karahashi, T.; Orimo, S. Halide-stabilized $LiBH_4$, a room-temperature lithium fast-ion conductor. *J. Am. Chem. Soc.* **2009**, *131*, 894–895. [CrossRef] [PubMed]
30. Matsuo, M.; Takamura, H.; Maekawa, H.; Li, H.W.; Orimo, S. Stabilization of lithium superionic conduction phase and enhancement of conductivity of $LiBH_4$ by LiCl addition. *Appl. Phys. Lett.* **2009**, *94*, 084103. [CrossRef]
31. Oguchi, H.; Matsuo, M.; Hummelshøj, J.S.; Vegge, T.; Nørskov, J.K.; Sato, T.; Miura, Y.; Takamura, H.; Maekawa, H.; Orimo, S. Experimental and computational studies on structural transitions in the $LiBH_4-LiI$ pseudobinary system. *Appl. Phys. Lett.* **2009**, *94*, 141912. [CrossRef]
32. Mosegaard, L.; Møller, B.; Jørgensen, J.E.; Filinchuk, Y.; Cerenius, Y.; Hanson, J.C.; Dimasi, E.; Besenbacher, F.; Jensen, T.R. Reactivity of $LiBH_4$: In situ synchrotron radiation power X-ray diffraction study. *J. Phys. Chem. C* **2008**, *112*, 1299–1303. [CrossRef]
33. Rude, L.H.; Groppo, E.; Arnbjerg, L.M.; Ravnsbæk, D.B.; Malmkjær, R.A.; Filinchuk, Y.; Baricco, M.; Besenbacher, F.; Jensen, T.R. Iodide substitution in lithium borohydride, $LiBH_4-LiI$. *J. Alloys Compd.* **2011**, *509*, 8299–8305. [CrossRef]
34. Langmi, H.W.; McGrady, G.S.; Liu, X.; Jensen, C.M. Modification of the H_2 desorption properties of $LiAlH_4$ through doping with Ti. *J. Phys. Chem. C* **2010**, *114*, 10666–10669. [CrossRef]
35. Li, Z.; Li, P.; Wan, Q.; Zhai, F.; Liu, Z.; Zhao, K.; Wang, L.; Lü, S.; Zou, L.; Qu, X.; et al. Dehydrogenation improvement of $LiAlH_4$ catalyzed by Fe_2O_3 and Co_2O_3 nanoparticles. *J. Phys. Chem. C* **2013**, *117*, 18343–18352. [CrossRef]
36. Ismail, M.; Zhao, Y.; Yu, X.B.; Dou, S.X. Effects of NbF_5 addition on the hydrogen storage properties of $LiAlH_4$. *Int. J. Hydrog. Energy* **2010**, *35*, 2361–2367. [CrossRef]
37. Atakli, Z.Ö.K.; Callini, E.; Kato, S.; Mauron, P.; Orimo, S.; Züttel, A. The catalyzed hydrogen sorption mechanism in alkali alanates. *Phys. Chem. Chem. Phys.* **2015**, *17*, 20932. [CrossRef] [PubMed]
38. Hoang, K.; Janotti, A; Van de Walle, C.G. Decomposition mechanism and the effects of metal additives on the kinetics of lithium alanate. *Phys. Chem. Chem. Phys.* **2012**, *14*, 2840–2848. [CrossRef] [PubMed]
39. Weng, Q.; Wang, X.; Wang, X.; Bando, Y.; Golberg, D. Functional hexagonal boron nitride nanomaterials: Emerging properties and applications. *Chem. Soc. Rev.* **2016**, *45*, 3989–4012. [CrossRef] [PubMed]

40. Lei, W.; Mochalin, V.N.; Liu, D.; Qin, S.; Gogotsi, Y.; Chen, Y. Boron nitride colloidal solutions, ultralight aerogels and freestanding membranes through one-step exfoliation and functionalization. *Nat. Commun.* **2015**, *6*, 8849. [CrossRef] [PubMed]
41. Liu, D.; He, L.; Lei, W.; Klika, K.D.; Kong, L.; Chen, Y. Multifunctional polymer/porous boron nitride nanosheet membranes for superior trapping emulsified oils and organic molecules. *Adv. Mater. Interfaces* **2015**, *2*, 1500228. [CrossRef]
42. Hu, S.; Lozada-Hidalgo, M.; Wang, F.C.; Mishchenko, A.; Schedin, F.; Nair, R.R.; Hill, E.W.; Boukhvalov, D.W.; Katsnelson, M.I.; Dryfe, R.A.W.; et al. Proton transport through one-atom-thick crystals. *Nature* **2014**, *516*, 227–230. [CrossRef] [PubMed]
43. Lei, W.; Zhang, H.; Wu, Y.; Zhang, B.; Liu, D.; Qin, S.; Liu, Z.; Liu, L.; Ma, Y.; Chen, Y. Oxygen-doped boron nitride nanosheets with excellent performance in hydrogen storage. *Nano Energy* **2014**, *6*, 219–224. [CrossRef]